Separation and Purification Technology 298 (2022) 121639

Contents lists available at ScienceDirect

Separation and Purification Technology

journal homepage: www.elsevier.com/locate/seppur

Key-study on plasma-induced degradation of cephalosporins in water: Process optimization, assessment of degradation mechanisms and residual toxicity

S. Meropoulis [a,b], S. Giannoulia [a], S. Skandalis [b], G. Rassias [b], C.A. Aggelopoulos [a,*]

[a] Laboratory of Cold Plasma and Advanced Techniques for Improving Environmental Systems, Institute of Chemical Engineering Sciences, Foundation for Research and Technology Hellas (FORTH/ICE-HT), GR-26504 Patras, Greece
[b] University of Patras, Chemistry Department, GR-26504 Patras, Greece

ARTICLE INFO

Keywords:
Cold atmospheric plasma
Wastewater treatment
Reactive oxygen and nitrogen species
Cephalexin
Cefazolin

ABSTRACT

Cephalosporins is a class of β-lactam antibiotics being widely used and often released uncontrollably in aquatic systems thus resulting in serious environmental contamination. In this work, we investigated for the first-time the degradation of cephalexin (CPX) and cefazolin (CFZ) by nanosecond-pulsed cold atmospheric plasma (NSP-CAP) using a multi-pin-to-liquid corona reactor, proposing special degradation pathways of both cephalosporins and assessing their residual toxicities. Increasing pulse voltage and frequency enhanced RONS concentration and energy input into the system both of which led to improved plasma-induced cephalosporin degradation efficiency, rate and energy yield, the latter being two orders of magnitude higher (0.84–1.37 g/kWh) than those reported for their photocatalytic degradation. O_2- and air-plasmas displayed superior performance compared to N_2-plasma due to the increased ROS concentration. The prevailing role of the short-lived ·OH and $^1O_2$ in the degradation process compared to the long-lived H_2O_2 and plasma electrons was confirmed. Nevertheless, the identical degradation efficiencies between air and oxygen indicated the possible significant contribution of some RNS (e.g. ONOOH/$ONOO^-$) generated due to nitrogen content in air-plasma. The plasma-induced degradants of CPX and CFZ were interrogated by UPLC/MS, comprehensive degradation maps were proposed and reduced cytotoxicity was demonstrated for both CPX and CFZ plasma-treated solutions. Given than CPX and CFZ are resistant to human (and other species) metabolism/degradation, this work supports that CAP constitutes arguably one of the most efficient remediation technologies to date.

1. Introduction

It is undeniable that antibiotics have a huge impact in our life and economy, as they constitute an indispensable medicinal arsenal to treat human diseases/infections and growth promoters/protectors in agri/aquaculture [1,2]. The extensive use of antibiotics, however, has resulted in environmental contamination, particularly in aquatic systems, due to the slow and limited biological degradation by living organisms [3–6].

The cephalosporins is a class of β-lactam antibiotics being used for a wide range of infections (e.g. pneumonia, urinary tract diseases, endocarditis, bone and stomach diseases) [7] and are the most commonly prescribed antibiotics worldwide; 50–70% of the antibiotics consumed belong to this family [8]. Among them, cefazolin (CFZ) is the most active against the gram-negative bacteria, while cephalexin (CPX) is effective against both gram-positive and negative pathogens [9]. The concentration of antibiotics in the environment varies from ng/L to mg/L for surface water/wastewater and pharmaceutical or animal-farm wastewater, respectively. Particularly for the commonly used cephalosporins their concentration extents up to several mg/L [10]. CPX and CFZ are resistant to human (and other species) metabolism/biodegradation and are excreted unchanged in the urine and feces, hence their environmental bioaccumulation from human, livestock and crop usage, is hard to control. Cephalosporins are highly resistant to biodegradation processes since apart from the easily hydrolyzed β-lactam ring they also possess a substrate site which is resistant to enzyme degradation and, in fact, acts as a competitive inhibitor [11]. In addition, bioaccumulation of antibiotics results in the development of resistant microbial

* Corresponding author.
E-mail address: caggelop@iceht.forth.gr (C.A. Aggelopoulos).

https://doi.org/10.1016/j.seppur.2022.121639
Received 6 May 2022; Received in revised form 28 June 2022; Accepted 29 June 2022
Available online 2 July 2022

pathogens which are classified as an important threat for ecosystems and modern societies, due to the associated heavy economic and health burden. Antimicrobial resistance (AMR) is responsible for an estimated number of 33,000 deaths per year in the EU, while the estimated costs due to AMR for the EU is approximately €1.5 billion per year [12]. The urgent need to address this serious concern is reflected in the intense focus and prioritization of EU actions towards this goal.

Advanced oxidation processes (AOPs) such as photocatalysis, ozonation and Fenton oxidation have been proposed towards the effective removal of antibiotics mainly due to the high reactivity of the species they generate [13–17]. Among AOPs, cold atmospheric plasma (CAP) has gained great attention, because of its advantages in high removal rate of organic contaminants and simple operation procedures, without requiring external additives [18–21]. The CAP-generated reactive oxygen and nitrogen species (RONS) such as $^1O_2$, ·OH, O, $\cdot O_2^-$, O_3, NO_2^-, NO_3^-, $ONOO^-$, H_2O_2, etc. possessing high oxidation potentials, are responsible for the rapid and cost-effective oxidation and mineralization of organic pollutants [18,22–24]. Regarding antibiotics, different CAP systems (e.g. DBDs, pulsed corona discharge, plasma jet) have been investigated towards the effective degradation of various classes of antibiotics including fluoroquinolones, sulfonamides and tetracyclines [25–31]. However, to the best of our knowledge, there is only one recent report on the degradation of cefixime by CAP [32] whereas no studies have been published on the degradation of other commonly used cephalosporins such as cephalexin and cefazolin.

The design of the plasma reactor is critical for the method's efficiency affecting active species generation, degradation efficiency and energy yield. Therefore, a significant number of efforts focus on the design of plasma reactors [33,34]. Among these, multi-pin corona discharge system has been proposed as an appropriate reactor to improve the discharge energy density requiring a lower voltage for the discharge formation [35]. In addition, several novelties have been also introduced to maximize the energy efficiency of plasma processes including the use of innovative power sources, especially those based on nanosecond pulsed generators [36–38], or the supplementary use of catalysts/additives to boost the generation of the reactive species [38–41]. Nevertheless, the use of catalysts introduces extra costs and recovery steps.

In the present study, we investigated for the first time the degradation of cephalexin and cefazolin by nanosecond pulsed CAP, using a multi-pin-to-liquid corona reactor, proposing special degradation pathways of both cephalosporins and assessing their residual toxicities; the by-products can sometimes be more harmful than the original mother molecule and therefore the determination of the intermediate products along with their potential toxicity assessment is crucial [42]. Based on the above-mentioned challenges, we used the high-energy efficient nanosecond pulses (NSP) to drive our system and we performed a detailed assessment of numerous factors influencing the process (treatment time, pulse voltage/frequency, energy yield, plasma gas, water properties, initial pollutant concentration) in order to find out the optimum operational conditions. In parallel, we explored thoroughly the degradation mechanisms involved in the plasma-induced degradation of CFZ and CPX through (i) identification of the various RONS in both the liquid and gas phase (ii) their relative impact/contribution in the degradation process, (iii) assessment of the water quality after air/oxygen/nitrogen NSP-corona treatment, (iv) identification of both CFZ and CPX degradation intermediates along with the suggestion of possible degradation pathways and (v) determination of their potential toxicity. Overall, we gained insight about the mechanisms that govern the degradation process under plasma conditions and we humbly believe that this effort provides the foundation for establishing a highly cost-effective remediation approach.

2. Experimental section

2.1. Materials and reagents

Cephalexin (CPX, $C_{16}H_{17}N_3O_4S$ M = 347.39 g·mol^{-1}), cefazolin (CFZ, $C_{14}H_{14}N_8O_4S_3$, M = 454.50 g·mol^{-1}), sodium pyruvate (SP), D-Mannitol (D-man), 2,2,6,6-Tetramethylpiperidine (TEMP) and monopotassium phosphate (MP) were all of analytical grade and purchased from Sigma Aldrich. The physicochemical properties of CPX and CFZ are summarized in section S1, Table S1.

2.2. Plasma device, treatment conditions and electrical measurements

The experimental-setup (Fig. 1a) consisted of a gas-liquid corona reactor, a nanopulsed power supply, a plasma characterization arrangement and a feeding gas system. The power supply (NPG-18/3500) was able to provide positive high-voltage pulses of very short nanosecond duration (rising time of ~4 ns and FWHM of ~15 ns) of regulated amplitude and frequency. The plasma characterization arrangement involved both an optical emission spectrometer (OES) and a discharge power measurement system comprised of a digital oscilloscope (Rigol MSO2302A) in connection to voltage (Tektronix P6015A) and current probes (Pearson electronics 2877). The corona reactor was of pin-to-plane geometry and comprised of a hollow quartz cylinder (diameter 60 mm, thickness 2 mm) serving as the water reaction tank. The HV electrode comprised of 13 stainless-steel pins was placed above the water surface (the distance between the tip of pins and water surface was ~ 2 mm) whereas a stainless-steel disc positioned at the bottom of the reaction tank and in direct contact with the aqueous phase, served as the grounded electrode.

For the preparation of the initial solution, 40 mg of CPX or CFZ was added in 1 L of water and stirred for 24 h (the dissolution was relatively fast since the solubility of CPX and CFZ in water is 10 mg/mL and 50 mg/mL, respectively). Afterwards, various concentrations of cephalosporins in water were prepared (ranged from 10 to 100 mg/L) and the treatment time varied from 1 to 20 min. In each experiment, 15 mL of aqueous solution was treated in the NSP-corona reactor. The experiments were performed at pulse voltages of 19.0, 21.4 and 24.2 kV, pulse frequencies of 100, 200 and 400 Hz under constant flow rate (i.e. 0.2 L min^{-1}) of different plasma working gases (air, oxygen and nitrogen). The degradation efficiency was determined by analyzing the samples right after the treatment and after retaining the treated solutions for 24 h in closed vials. A slight increase on the degradation efficiency was recorded when the samples were kept in closed vials for 24 h indicating that the residual long-lived species further reacted with the cephalosporins (data not shown). Thus, all treated solutions were stored at ~20 °C for 24 h to allow for residual long-lived plasma RONS sufficient time to quench by reacting with the cephalosporins and their degradants. Experiments were conducted in duplicate or triplicate and the mean values along with their error bars are reported. In all Figures the continuous line serves as a guide to the eye for the scattered points. Details regarding the electrical measurements, $V(t)$-$I(t)$ signals synchronization, calculation of instantaneous power and mean power dissipated in the reactor can be found in our previous work [38].

2.3. Chemical analysis of water samples

To explore the degradation and mineralization of cephalosporins by NSP-corona, the treated water samples were analyzed by UV–Vis spectroscopy, HPLC and TOC analysis. HPLC details are given in S3, whereas the quantification of CPX and CFZ degradation by UV–Vis was assessed using a Shimadzu UV-1900 spectrophotometer by monitoring the peak absorbance at 262 and 272 nm, respectively. Solutions with known concentrations of CPX and CFZ were prepared, and the subsequent calibration curve was designed for UV/Vis, HPLC and TOC analysis. HPLC analysis was used to quantify the residual concentrations of the

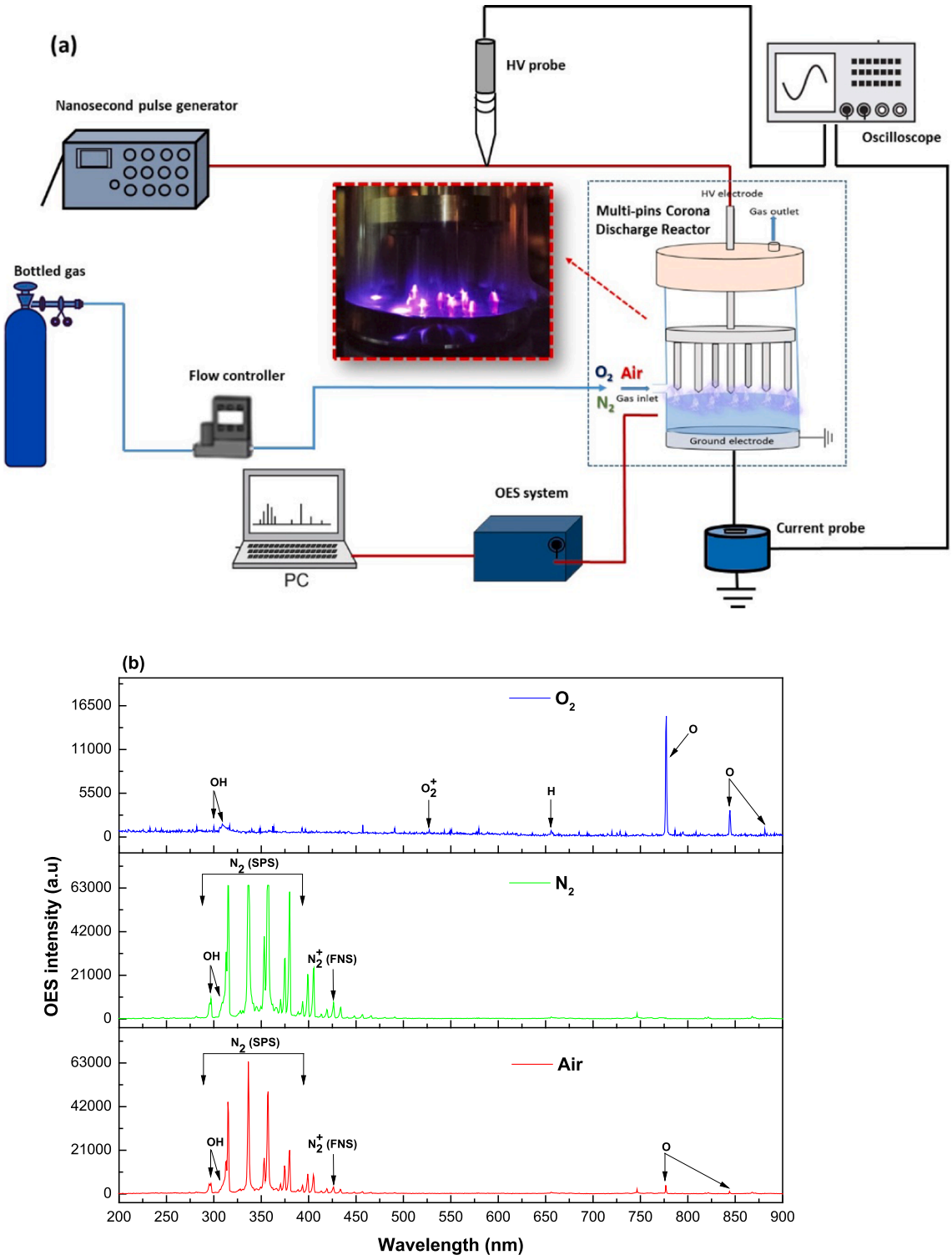

Fig. 1. (a) Schematic diagram of the experimental apparatus used to treat cephalosporin antibiotics-polluted water by NSP-corona plasma and (b) Optical emission spectra of the NSP-corona reactor operated with oxygen, nitrogen and air gases ($V = 24.2$ kV, $f = 200$ Hz).

parent CPX and CFZ molecules whereas UV–Vis spectroscopy was adopted to investigate both the oxidation of parent molecules along with those with similar conjugate structures which absorb at near wavelengths [32]. The comparison between HPLC, UV–Vis and TOC analysis towards CPX degradation are shown in section S4, Fig. S2. Unless otherwise stated, the pollutant degradation efficiency shown in the Figures of this study was based on UV/Vis spectroscopy. The total organic carbon (TOC) content in the water samples before and after NSP treatment was quantified using a Shimadzu TOC analyzer (TOC-VCSH).

The degradation efficiency (%) was calculated as:

$$D(\%) = \left[\frac{C_0 - C_f}{C_0}\right] \times 100 \quad (1)$$

where C_0 and C_f are the CPX and CFZ concentrations before and after plasma treatment, respectively. The degradation kinetics were determined using the pseudo-first order equation:

$$ln\left(\frac{C_0}{C_f}\right) = kt \quad (2)$$

where k is the kinetic constant whereas the energy yield (Y; g/kWh), was calculated by the expression:

$$Y = \frac{C_0 VD}{Pt} \quad (3)$$

where V is the volume of treated water, D the degradation efficiency, P the average power dissipated in the reactor and t refers to the treatment time.

2.4. Measurement of plasma reactive species and use of scavengers

The major gaseous plasma-induced species were detected with the aid of a fiber-optic spectrometer (AvaSpec-ULS2048CL-EVO) that was used to record the optical emission spectra of the NSP discharge from 200 to 900 nm. Regarding the quantification of plasma species in the aqueous phase, a Quantofix® Relax device (Macherey-Nagel, GmbH) along with test strips, certified and calibrated by the supplier, were used to determine the concentration of H_2O_2, nitrate ions (NO_3^-) and nitrite ions (NO_2^-). Furthermore, in order to explore the role of several plasma species in the degradation of antibiotics in the current NSP system, scavenging experiments were conducted by adding sodium pyruvate (SP), monopotassium phosphate (MP), D-Mannitol (D-man) and 2,2,6,6-Tetramethylpiperidine (TEMP) to trap H_2O_2, e_{aq}^-, $^{\cdot}OH$ and $^1O_2$, respectively. The concentration of each scavenger in water was 1 mmol/L. The action efficiency of plasma species was calculated as:

$$\varphi = \left[\frac{D_0 - D_1}{D_0}\right] \times 100\% \quad (4)$$

where D_0 and D_1 are the degradation of antibiotics in the absence and presence of the corresponding scavenger, respectively.

2.5. UPLC/MS analysis of water samples and degradation pathway study

The degradation intermediates of the parent CPX and CFZ molecules were identified using UPLC/MS. The UPLC/MS (ESI) analysis was conducted in a Thermofischer system equipped with Thermofisher 27101–152130 C_{18} (150 mm × 1.50 mm, 2.1 mm) column and the detection of cephalosporins and their degradants were monitored at 190–800 nm. A gradient method was applied for the mobile phase using water (Solvent A) and acetonitrile (Solvent B) each containing 0.05 w/w % trifluoroacetic acid, at 40 °C and with the flow rate set to 0.1 mL/min.

2.6. Cytotoxicity assessment

Cephalosporins cytotoxicity was assessed towards three different human cells; MCF-7 and MDA-MB-231 cells representing low and high metastatic breast cancer cells respectively, and U251MG glioblastoma cells. All cell lines originally obtained by the ATCC (USA), were seeded in a 24-well plate (5x104 cells per well) and incubated at 37 °C and 5 % (v/v) CO_2 in a humidified incubator for 24 h. The medium was then replaced with serum free medium and the cells were starved overnight (16–18 h). Next day, 100 μL of fresh medium (serum free) containing 10 μL of CPX or CFZ solutions (before and after plasma treatment) was added and the cells were incubated for 24 h. Cells were washed with cold PBS and stained with 0.5% (w/v) crystal violet solution in 20 % (v/v) methanol/distilled water for 20 min at 37 °C with 150 oscillations on a bench rocker. Staining solution was removed and the excess dye was washed away. Stained cells were left to dry for 24 h at room temperature. Next, methanol was added to each well and the cell-bound dye was retrieved after 20 min incubation of the plate at 150 oscillations on a bench rocker. Following the incubation, optical density of each well was measured at 570 nm using a TECAN photometer, utilizing Magellan 6.

3. Results and discussion

3.1. Electrical and optical characterization of the NSP plasma discharge

Typical instantaneous voltage and current waveforms over the pulse duration are shown in section S2, Fig. S1. After the main pulse, a sequence of smaller pulses is observed in agreement with previous studies using nanopulses of very short rising time [43]. The instantaneous pulse current is quite high (~100-150 A) which is up to three orders of magnitude higher compared to that measured in AC-driven DBD reactors [44]. Thus, the instantaneous power of the present NSP system was ~2.5 MW (section S2, Fig. S1); however, the mean discharge power was calculated between ~1.6 and 5.1 W (depending on the applied pulse voltage/frequency) due to the very short duration of the main pulse (section S2, Table S2). The combination of the extremely high instantaneous power and the quite low mean power is the key-factor of the enormously high energy efficiency reported for the NSP-driven plasma reactors [45]. In other words, the NSP discharge provides instantly high concentrations of reactive species (high instantaneous power), while in parallel requiring low mean power consumption.

Optical emission spectra were recorded at the gas-liquid interface of the NSP reactor under the various plasma working gases to detect various excited molecular and atomic plasma RONS (Fig. 1b). Under O_2-plasma, the main species identified include the following ROS: ·OH emission peak at 309 nm acting as strong oxidant and precursor of H_2O_2 generation [46], O emission lines at 777 and 844 nm [47], and dioxygen cation O_2^+ line at 527 nm [48]. ·OH, ·H and O are produced by the energetic collisions of electrons with water and O_2, respectively whereas O_2^+ through electron impact ionization of O_2:

$$H_2O + e^- \rightarrow {\cdot}H + {\cdot}OH + e^- \quad (5)$$

$$H_2O + e^- \rightarrow 2{\cdot}H + O + e^- \quad (6)$$

$$O_2 + e^- \rightarrow 2O + e^- \quad (7)$$

$$O_2 + e^- \rightarrow + 2e^- \quad (8)$$

Under N_2-plasma, the main observed emission peaks originated from the second positive system of excited molecular nitrogen molecules (N_2 SPS) in the range 315–405 nm through electron impact excitation. Emission peaks observed from 297 nm to 311 nm are attributed to ·OH whereas N_2^+ emissions at 393 and 427 nm are originated from electron impact ionization of excited nitrogen molecules [38].

Under air-plasma the spectrum is dominated by both ROS and RNS: N_2 SPS, N_2^+, ·OH and low intensity peaks of O were observed (Fig. 1b) generated through the reactions:

$$H_2O + N_2 \rightarrow {\cdot}H + {\cdot}OH + N_2 \quad (9)$$

$$O_2 + N_2 \rightarrow 2O + N_2 \quad (10)$$

$$N_2 + O \rightarrow {\cdot}NO + {\cdot}N \quad (11)$$

$$N_2^* + e^- \rightarrow N_2^+ + 2e^- \quad (12)$$

NO gamma emission lines, normally detected in the range 230–260 nm [49], were very weakly observed possibly due to NO radical quenching by oxygen molecules and oxygen atoms [50]. The different OES spectra between the various plasma gases result in different RONS generated inside the aqueous phase affecting the degradation of cephalosporin antibiotics (see below section 3.3).

3.2. Effect of discharge parameters

3.2.1. The impact on RONS concentration and degradation efficiency

The parametric analysis of the present study is based on UV–Vis analysis which secures the oxidation of parent CPX and CFZ molecules along with the oxidation of their conjugate molecules.

It is well-known that plasma operating parameters such as pulse voltage and repetition rate is of crucial importance since it affects substantially the generation of plasma RONS and subsequently the degradation and energy efficiency of the whole process [18]. In general, the generation of plasma RONS is increased as pulse voltage and pulse frequency is increased. However it is noteworthy that the beneficial increase of species generation with pulse frequency usually reaches an optimum value, while extra discharge power at higher pulse frequencies causes mainly heating of the reactor [51]. The effect of pulse frequency on CPX degradation efficiency at various NSP treatment times is depicted in Fig. 2a. Naturally, an increase from 100 to 200 Hz had a positive effect on CPX degradation whereas further increase to 400 Hz improved marginally the degradation efficiency. After 20 min of NSP treatment, CPX had been degraded by 77.2, 99.0 and 99.3% at pulse frequency 100, 200 and 400 Hz respectively, while the corresponding pseudo-first order kinetic constants were 0.09, 0.23 and 0.26 min^{-1} (section S5, Fig. S3a).

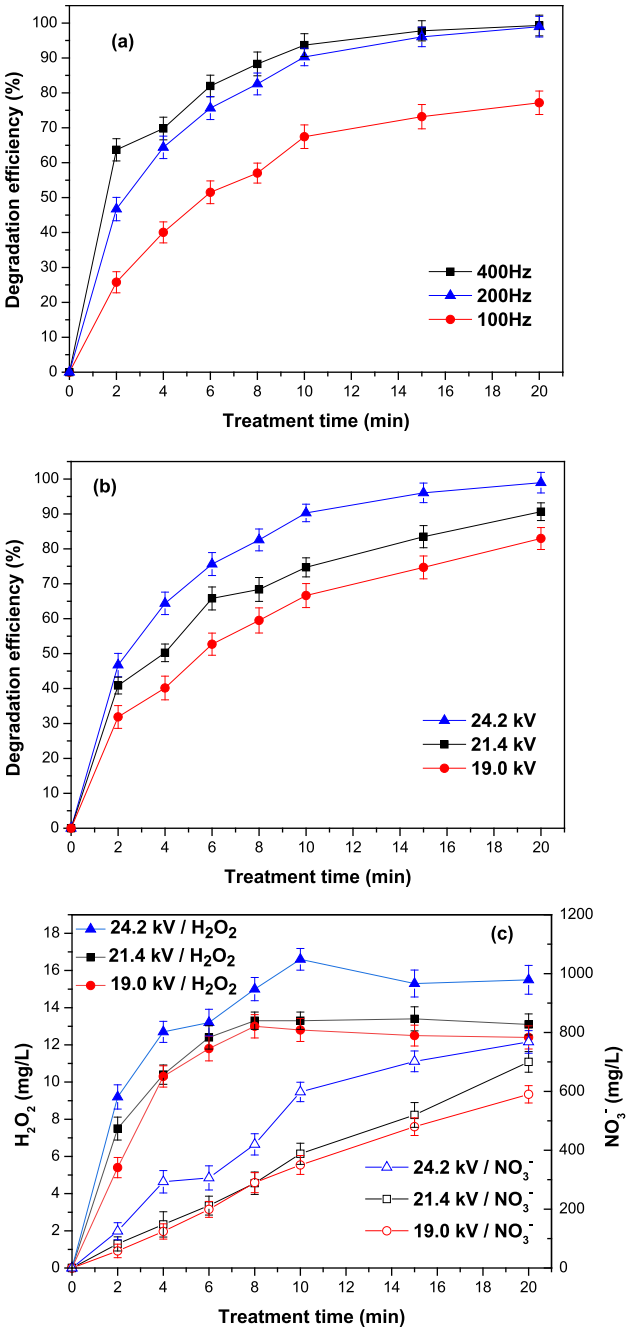

Fig. 2. Cephalexin degradation efficiency as a function of plasma treatment time for different (a) pulse frequencies at 24.2 kV and (b) pulse voltages at 200 Hz (carrier gas: air; initial pollutant concentration: 40 mg/L); (c) Concentration of H_2O_2 and NO_3^- in MilliQ water as a function of NSP-corona treatment time for different pulse voltages at 200 Hz (carrier gas: air).

Similar to the effect of pulse frequency, we observed an enhancement of CPX degradation efficiency and degradation rate with pulse voltage (Fig. 2b). After 20 min of NSP plasma treatment at 200 Hz, CPX degraded by 82.9% at 19.0 kV (1.63 W) and by 90.6% and 99.0% at 21.4 kV (2.16 W) and 24.2 kV (2.72 W), respectively. The first-order degradation kinetic constant was also improved being 0.09, 0.13 and 0.23 min^{-1} at 19.0, 21.4 and 24.2 kV, respectively (section S5, Fig. S3a).

In general, the improvement of pollutant degradation with pulse voltage and pulse repetition rate is attributed to the increased intensity of the UV and plasma RONS. The concentration of H_2O_2 and NO_3^- in the aqueous solution was enhanced at increased pulse voltages which supports the greater CPX degradation efficiency/rate. After 20 min of NSP treatment, the concentration of H_2O_2 in water was 12.4, 13.1 and 15.5 mg/L at pulse voltage 19.0, 21.4 and 24.2 kV, respectively. Similarly, NO_3^- concentration was increased from 590 to 700 and 768 mg/L with pulse voltage increasing from 19.0 to 21.4 and 24.2 kV, respectively (Fig. 2c).

Conclusively, enhanced power input in the NSP-corona reactor at higher pulse voltage and frequency led to increased RONS concentration in the aqueous solution which in turn improved the plasma-induced CPX degradation efficiency and rate. This agrees with previous reports on the degradation of antibiotics ciprofloxacin, enrofloxacin and trimethoprim either in soil or in water using high voltage nanopulses to drive the degradation process [38,44,52].

3.2.2. *The impact on energy efficiency*

In order to thoroughly evaluate the overall performance of the NSP-corona reactor towards the degradation of cephalosporins, we calculated the process energy yield as a function of pollutant degradation under the various pulse voltages and frequencies (Fig. 3a and b). For a given pollutant degradation efficiency, the energy yield increased with increasing pulse voltage (Fig. 3a) and pulse frequency from 100 to 200 Hz, and declined at pulse frequency of 400 Hz (Fig. 3b). On the one hand, the increase of energy yield with pulse voltage and frequency (up to 200 Hz) is due to the higher applied electric field and power dissipated in the plasma reactor (section S2, Table S2) resulting in enhanced concentration of plasma RONS (Fig. 2c). On the other hand, the lower energy yield observed at 400 Hz (Fig. 3b) indicates that the enhanced power dissipated in the system at higher pulse frequencies (section S2, Table S2) may be wasted as heat in the reactor and power supply components and/or results in excessive production of H_2O_2 and nitrite/nitrate ions which begin to act as scavengers for ·OH and O_3 thus decreasing the pollutant degradation efficiency [37,53]. Balancing plasma treatment time, process energy yield, pollutant degradation efficiency and rate, we recommend 24.2 kV and 200 Hz as the optimum plasma conditions of the present NSP-corona reactor. Under these conditions, CPX (with initial concentration in water at 40 mg/L) was degraded by 96.1% after 15 min of plasma treatment with energy yield 0.85 g/kWh, whereas an even higher energy yield (i.e. 1.37 g/kWh) was calculated at 100 mg/L initial CPX concentration (see below section 3.4).

We compared the performance and energy yield of the NSP-corona with other AOPs towards cephalosporins degradation (Table 1). Various studies using TiO_2, N-doped TiO_2, nano α-Fe_2O_3/ZnO, N-TiO_2/$ZnFe_2O_4$/zeolite and CdSe quantum dots photocatalysts under UV and/or UV–Vis irradiation are less or similarly effective in degrading cephalosporin antibiotics such as cephalexin, cefazolin and cefixime. Nevertheless, all these studies reveal a much lower energy yield (about two orders of magnitude) compared to that achieved with our NSP-corona system reported hereby (Table 1). Interestingly, the extremely

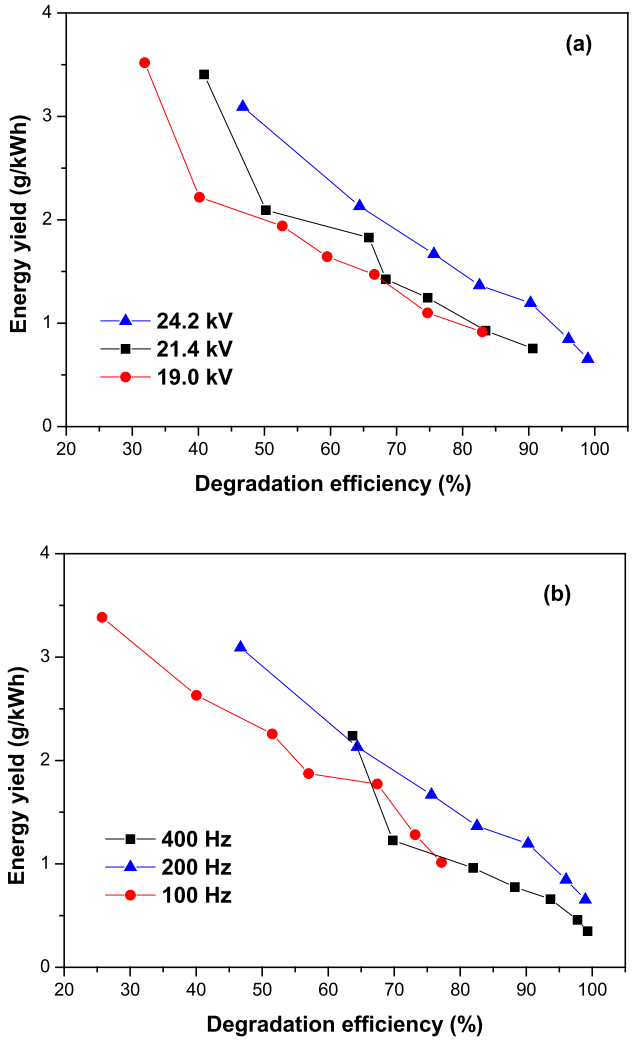

Fig. 3. Energy yield as a function of cephalexin degradation efficiency at various (a) pulse voltages at 200 Hz and (b) pulse frequencies at 24.2 kV (carrier gas: air; initial pollutant concentration: 40 mg/L).

high energy yield of the presently described NSP-corona system (in the g/kWh range) is very similar to that achieved using a microplasma bubble reactor as a means to improve process energy yield through the enhancement of RONS mass transfer from the gas to liquid phase [32]. In our study where a typical gas-liquid corona system is used, the remarkable energy yield achieved is due to the extremely high instantaneous power (~2–3 MW) of nanosecond duration (~4 ns) that is initially directed in the multi-pin-to-liquid corona reactor (section S2, Fig. S1) which results in high current density and mean electron energies hence RONS generation of high concentration even at low mean discharge power (section S2, Table S2).

It is noteworthy though that in many studies existing in the literature, larger volumes have been investigated, and therefore a direct comparison of the energy yield may be insecure. However, the extremely high energy-efficient and almost complete degradation of cephalosporins in this lab-scale reactor foretells a promising method for the cost-effective remediation of antibiotic-polluted wastewater in larger volumes as well. Considering that the optimization of the process in the lab-scale is the mandatory critical step before the optimization in larger scale, the outcomes obtained from the present study will act as the steppingstone for further research. More specifically, the main task towards the up-scaling of the present lab-scale reactor is to maintain its effectiveness in terms of degradation and energy efficiency. To that end, our next steps involve the design and construction of a pilot-system

Table 1
Comparison of cephalosporins degradation in water by various AOPs.

Method	Pollutant	D (%) /time	V (ml)	Y (g/kWh)	Ref
NSP-corona	Cephalexin, 40 mg/L	96.1/ 15 min	15	0.85	This study
NSP-corona	Cefazolin, 40 mg/L	95.2/ 15 min	15	0.84	This study
NSP-corona	Cephalexin, 100 mg/L	82.5/ 20 min	15	1.37	This study
Underwater plasma bubbles	Cefixime, 100 mg/L	94.8/ 30 min	–	1.5	[32]
nano α-Fe_2O_3/ZnO UV photocatalysis	Cefixime, 10 mg/L	99.1/ 127 min	300	0.022	[54]
TiO_2 UV photocatalysis	Cefazolin, 4.5 mg/L	53/60 min	600	0.036	[55]
N-doped TiO_2 UV photocatalysis	Cefazolin, 4.5 mg/L	76/50 min	600	0.062	[55]
N-TiO_2/$ZnFe_2O_4$/ zeolite UV–Vis Photocatalysis	Cephalexin, 100 mg/L	74/ 120 min	250	0.023	[56]
ZnO nanowires (40 mg/L) Solar photocatalysis	Cephalexin, <0.1 mg/L	96/25 min	–	–	[57]
CdSe quantum dots (500 mg/L) UV photocatalysis	Cephalexin, 15 mg/L	70.3/ 60 min	100	–	[58]

comprising of multiple HV multi-pin electrodes treating a larger amount of polluted water; the conceptual design of a "multiple HV multi-pin electrodes" pilot-scale corona reactor is presented in Fig. S5. Keeping the lab-scale reactor parameters (electrode gap, water thickness, etc.) constant and based on the optimization results of the present study, it is anticipated that each one of the HV electrodes will effectively treat 15 mL of contaminated water requiring 2.72 W when the system operates at $V = 24.2$ kV and $f = 200$ Hz (Table S2). For instance, 150 mL of contaminated water is expected to be effectively treated within 15-20 min in a pilot-scale plasma reactor comprised by ten (10) HV multi-pin electrodes with the power consumption being 27.2 W. Therefore, for each additional treated water volume (by using an extra HV multi-pin electrode), an analogous increase of power/energy requirement is anticipated, retaining the energy efficiency of the process. The number of HV electrodes will be adjusted based on the maximum power of the available HV generator. For the treatment of even larger water volumes, the parallel operation of the above-mentioned pilot-scale corona reactors will be required.

3.3. *Effect of plasma carrier gas on CPX degradation and assessment of plasma-treated water*

3.3.1. *Effect on degradation efficiency*

The plasma reactive species chemistry can be tuned by altering the gas used [59]. In particular, the plasma working gas has been found to affect the degradation of antibiotics both in NSP-DBD and microplasma bubble (MPB) reactors suggesting that different kinds of RONS and/or densities thereof are generated with different feeding gases [32,38]. In order to shed light on the gas-induced densities of the generated RONS and their impact on the degradation efficiency, we investigated the effect of three different plasma working gases (air, O_2 and N_2) on CPX degradation along with a detailed examination of the transient evolution of the plasma-induced H_2O_2, NO_2^- and NO_3^- as well as the pH variation in the treated water.

The progress of cephalexin degradation under the various gas atmospheres is depicted in Fig. 4a. CPX degradation was higher when oxygen and air plasmas were used whereas CPX was less degraded under nitrogen plasma. In particular, >99.9% and 96.1% CPX degradation was achieved after 20 min of oxygen and air plasma treatment, respectively

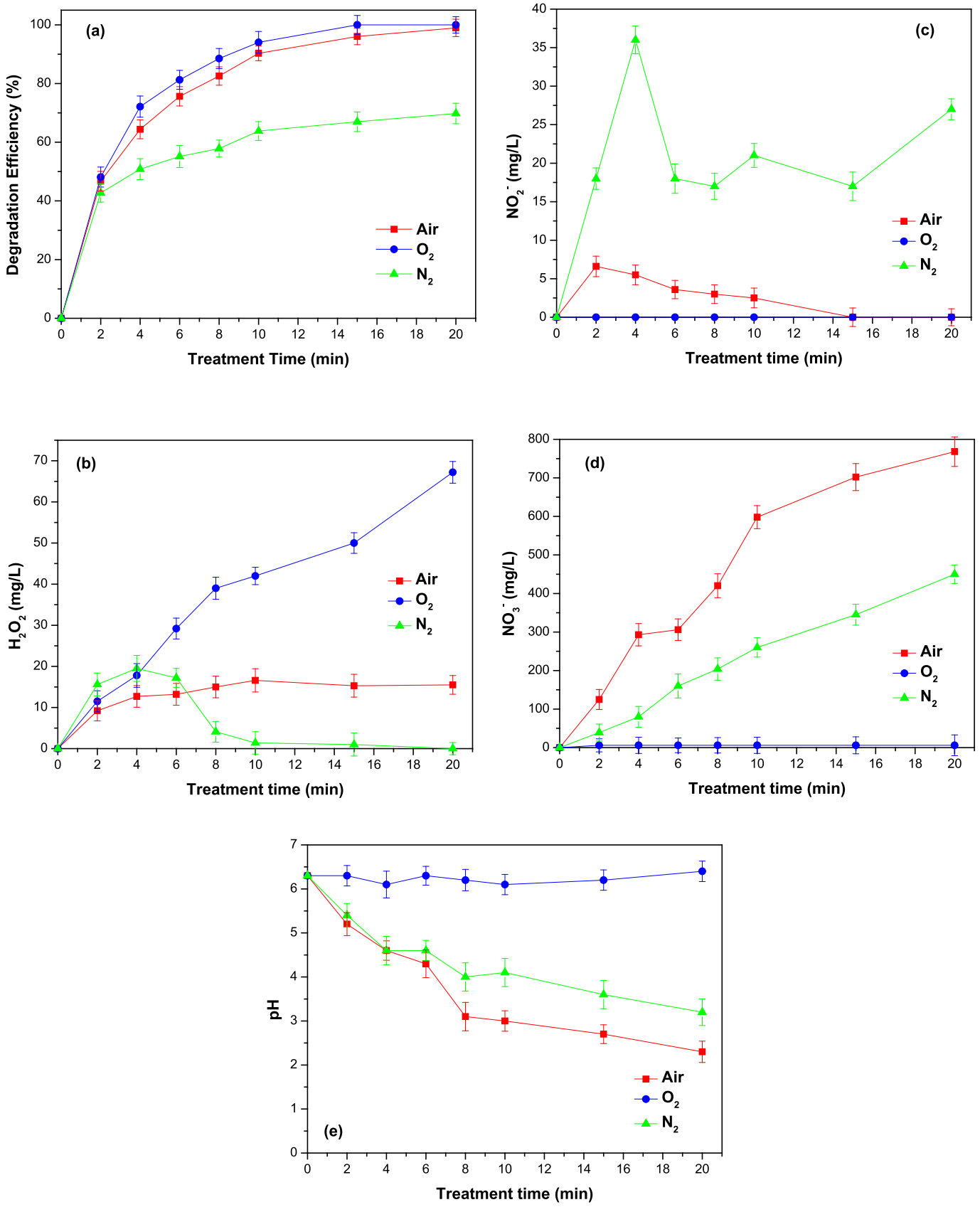

Fig. 4. The effect of plasma carrier gas on (a) cephalexin degradation efficiency; (b) H_2O_2 concentration; (c) NO_2^- concentration; (d) NO_3^- concentration and (e) solution pH (pulse voltage: 24.2 kV; pulse frequency: 200 Hz).

whereas nitrogen plasma was able to degrade CPX by 69.8% at the same time interval. The pseudo first-order kinetics are depicted in section S5, Fig. S3b, with the corresponding kinetic constants calculated as 0.28 min^{-1}, 0.23 min^{-1} and 0.08 min^{-1} for O_2, air and N_2 plasma, respectively. The superiority of oxygen and air plasma towards CPX degradation could be attributed to the prevailing role of plasma-induced ROS in comparison to RNS, given that an increased production of ROS is expected under O_2-containing atmospheres compared to N_2 gas [30]. Discussion on the temporal concentrations of the RONS generated under the various plasma atmospheres follows.

3.3.2. *Effect on H_2O_2, NO_2^-, NO_3^- concentration and solution pH of plasma-treated water*

The aforementioned assumption is fully supported by the measured concentration of H_2O_2, (a typical plasma-induced ROS in aqueous solutions) under the different gas atmospheres. During NSP treatment, the impact of high energy electrons on water molecules results in the generation of ·OH and H_2O_2 (Eqs. (13)-(15)) [60,61]:

$$H_2O + e^- \rightarrow \cdot H + \cdot OH + e^- \quad (13)$$

$$\cdot OH + \cdot OH \rightarrow H_2O_2 \quad (14)$$

$$e^- + H_2O_2 \rightarrow OH^- + \cdot OH \quad (15)$$

As shown in Fig. 4b, the H_2O_2 concentration was identical under short plasma treatment times for all gases. Nevertheless, at prolonged NSP treatment times, H_2O_2 concentration was higher under oxygen plasma compared to air plasma, whereas under nitrogen plasma the H_2O_2 concentration was the lowest measured and essentially vanished after 8 min of treatment which is consistent with ROS quenching by RNS (e.g. NO_2^-) [38,62]. After 20 min of NSP treatment, H_2O_2 concentration in aqueous solution was zero, 15.5 and 67.2 mg/L at nitrogen, air and oxygen plasma, respectively. The higher H_2O_2 concentration along with the oxygen species detected through OES in the gas phase of oxygen and air plasma (Fig. 1b) is indicative of the increased ROS concentration under O_2-containing atmospheres resulting in enhanced CPX degradation (Fig. 4a).

Besides increased ROS concentration and higher CPX degradation efficiency and rate, another advantage of using O_2 as a plasma carrier gas is the avoidance of undesirable by-product formation in the treated water (i.e. nitrite/nitrate) which also results in its acidification [30,37]. It is well known that RNS (i.e. NO and NO_2), generated in the plasma gas phase react with water molecules at the surface of the solution generating other chemical species including nitrites (NO_2^-) and nitrates (NO_3^-):

$$2\ NO_2\ (g) + H_2O \rightarrow NO_2^-\ (aq) + NO_3^-\ (aq) + 2H^+\ (aq) \quad (16)$$

Fig. 4c and Fig. 4d depict the concentration of nitrite and nitrate under the various plasma working gases, respectively. Under O_2-plasma, no gaseous NO/NO_2 are generated in the plasma gas phase resulting in negligible NO_2^- and NO_3^- concentrations in plasma treated water. Therefore, for all O_2-plasma treatment times the pH of the aqueous solution remained constant at ~ 6.3 (Fig. 4e). In contrast, in air- and N_2-plasma treated aqueous solutions, the pH decreased from 6.5 to 3.2 and 2.3 under nitrogen and air atmosphere, respectively after 20 min of NSP treatment; significant concentrations of both NO_2^- and NO_3^- were measured. As shown in Fig. 4c, the concentration of NO_2^- was higher for N_2- compared to air-plasma. For N_2-plasma, NO_2^- concentration increased up to 36 mg/L and decayed to 27 mg/L at the end of plasma treatment whereas for air-plasma it increased up to 6.6 mg/L and vanished after 15 min of treatment. Compared to NO_2^-, a much higher NO_3^- concentration was observed for both nitrogen and air plasmas (Fig. 4d) being an increasing function of NSP treatment time; its maximum value was measured at the end of treatment and found equal to 768 mg/L and 450 mg/L for air- and N_2-plasma, respectively. The relative concentration profiles of NO_2^-/NO_3^- is consistent with NO_2^- being an intermediate in NO_3^- formation [63] and responsible for ·OH and O_3 quenching through the following reactions [38,62]:

$$NO_2^- + \cdot OH \rightarrow NO_3^- + \cdot H \quad (17)$$

$$NO_2^- + O_3 \rightarrow NO_3^- + O_2 \quad (18)$$

Therefore, in contrast to O_2-plasma, the gradual decrease of solution pH under nitrogen and air plasmas is attributed to the generation of the aforementioned plasma RNS (e.g. NO_2^-, NO_3^-, ONOOH). The required O_2 for the gaseous NO/NO_2 generation, under N_2-plasma, and the subsequent NO_2^-/NO_3^- formation inside the water phase was possibly provided either by O_2 impurities dissolved in traces into the solution or by gas bubbles formed inside the water during the plasma treatment [63].

Thus, for O_2-plasma where the initial neutral pH is preserved, the collisions of plasma electrons with water molecules generate ·OH which dimerize to form H_2O_2 (reactions (13) and (14)) leading to increased concentration of these species whereas in the acidic conditions gradually established in the air- and N_2-plasma, the nitrite anions destroy H_2O_2 according to reaction (19) therefore the concentration of H_2O_2 attenuates (Fig. 4b). The higher CPX degradation efficiency under O_2-plasma and air-plasma is therefore attributed to the increased ROS concentration compared to N_2-plasma where the generated RNS may prevent the generation of ROS and/or scavenge them.

On the other hand, peroxynitrous acid (ONOOH), which is the -conjugate acid of peroxynitrite ($ONOO^-$), has been found to be produced from the reaction between NO_2^- and H_2O_2 in acidic conditions [64,65]:

$$NO_2^- + H_2O_2 + H^+ \rightarrow ONOOH + H_2O \quad (19)$$

Peroxynitrite and peroxynitrous acid (and/or other RNS) may also be contributing to CPX degradation since the > 4-fold increase in H_2O_2 production in O_2- compared to air-plasma does not translate in analogous degradation efficiency or rate (Fig. 4a and 4b). This suggests that the inhibitory effect (against ROS) exerted by certain RNS (e.g. NO_2^-) produced from the nitrogen present in the air-plasma, is by far outweighed by the oxidizing power of other long-lived RNS (e.g. HNO_3/NO_3^-) and short-lived ones (e.g. ONOOH/$ONOO^-$). A detailed report on the plasma-generated RNS inside the liquid phase can be found in [66]. Evidently, in this way, the nitrogen content in air-plasma provides a significant net benefit to the degradation process to the point that ultimately the degradation efficiencies between O_2- and air-plasma processes are essentially identical.

Notwithstanding the superiority of O_2-plasma in terms of improving the degradation rate/efficiency and limiting the formation of undesirable RNS-related by-products, subsequent experiments were conducted using air as the plasma gas due to its lower cost and similar CPX degradation efficiency.

3.4. *Effect of initial pollutant concentration and water matrix on degradation*

In addition to NSP treatments at initial CPX concentration of 40 mg/L, we performed experiments at both lower and higher initial CPX concentrations (i.e. 10, 20 and 100 mg/L) (Fig. 5a) wanting to cross-examine the process efficiency in both heavily and more realistic concentration of antibiotic contamination in water bodies. In real-life conditions, antibiotic contamination up to several mg/L has been reported in surface/fresh waters and pharmaceutical/animal wastewater [30,67]. When initial CPX concentrations of 10, 20, 40 and 100 mg/L were used, and each treated for 4 min under the optimized NSP conditions (pulse frequency 200 Hz, pulse voltage 24.2 kV), CPX degradation was almost complete (i.e. 99.7%) with the 10 mg/L sample while with the more concentrated samples CPX degradation decreased respectively to 75.9, 64.4 and 42.4%. Extending the treatment time to 20 min caused complete degradation of CPX (>99.9%) in the samples with initial concentrations of 10 and 20 mg/L whereas degradation reached to 99.0% and 82.5% with the 40 and 100 mg/L samples (Fig. 5a). Furthermore, the

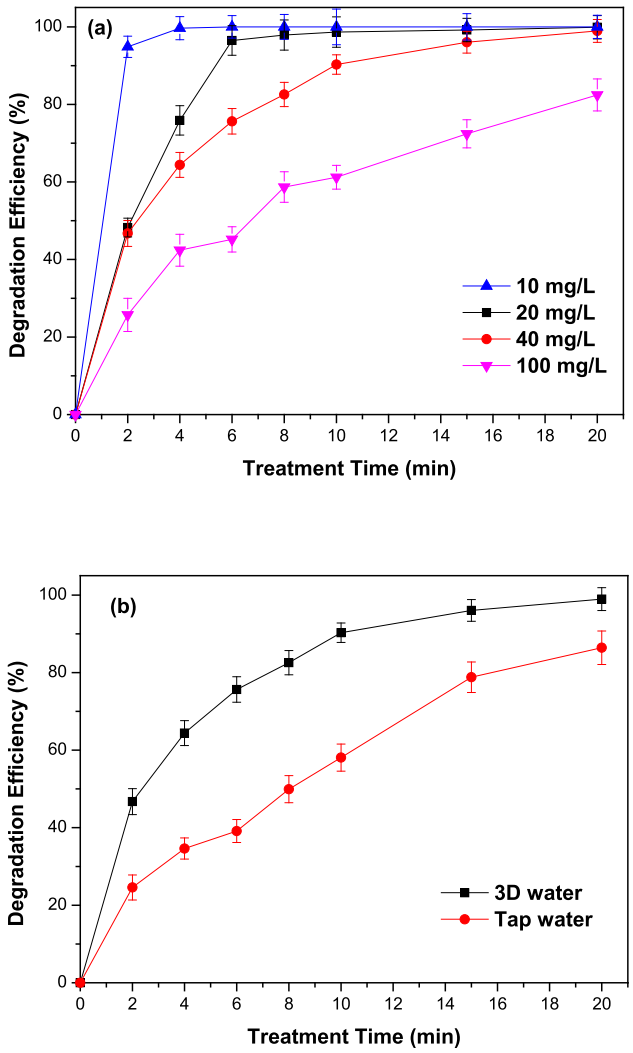

Fig. 5. Cephalexin degradation efficiency as a function of NSP-corona treatment time for different (a) initial pollutant concentrations and (b) water matrices for initial pollutant concentration 40 mg/L (pulse voltage: 24.2 kV; pulse frequency: 200 Hz; carrier gas: air).

degradation kinetic constant decreased accordingly from 1.43 (10 mg/L) to 0.37 (20 mg/L), 0.23 (40 mg/L) and 0.09 min^{-1} (100 mg/L) (section S5, Fig. S3c).

The reduced CPX degradation at higher pollutant concentration can be rationalized by the fact that more CPX molecules exist thus decreasing the ratio of plasma RONS per CPX molecule in agreement with previous studies [32,68]. Nevertheless, the exceptional efficiency of the NSP process at CPX concentrations of 10–20 mg/L is of great importance because these are within the CPX concentrations found in real-life antibiotic-contaminated water effluents.

With the aim to examine the NSP plasma effectiveness at scenarios closer to real life conditions, we also explored the effect of water matrix on CPX degradation. A comparison of CPX degradation in triply distilled (3D) and tap water is depicted in Fig. 5b. CPX degradation was slower in tap water compared to that in 3D water with the corresponding degradation kinetic constants being 0.23 (3D water) and 0.10 min^{-1} (tap water) (section S5, Fig. S3d). Nevertheless, after 20 min of NSP treatment, a respectable CPX degradation in tap water was achieved (i.e. 86.5%).

The decrease in CPX degradation efficiency in real water samples is attributed to the various species (molecules and ions) present in tap water which affect its pH and conductivity [69]. Each and every entity present in the water will compete with the pollutant for reaction with the plasma species thus less RONS available for the desired degradation reaction.

3.5. Relative contribution of plasma RONS to the degradation process

In order to assess the individual contribution of several key RONS to the degradation process we decided to dial out each contribution by using species-specific scavengers. Based on literature reports and our previous experience [37,70], we selected sodium pyruvate (SP), monopotassium phosphate (MP), D-Mannitol (D-man) and 2,2,6,6-Tetramethylpiperidine (TEMP), as suitable scavenging agents for H_2O_2, e^-_{aq}, ·OH and $^1O_2$ respectively. Obviously, CPX degradation efficiency decreased in the presence of all examined scavengers (Fig. 6a). In particular, after 20 min of NSP plasma treatment, CPX degradation efficiency decreased from 99.0% (no scavenger) to 68.8%, 72.1%, 87.3% and 90.7% in the presence of D-man, TEMP, SP and MP, respectively and the corresponding pseudo-first order kinetic constants were decreased accordingly from 0.23 (no scavenger) to 0.06, 0.07, 0.12 and 0.14 min^{-1} (section S5, Fig. S3e).

In addition to the attenuation of CPX degradation efficiency and kinetics in the presence of scavengers, the action efficiency of each

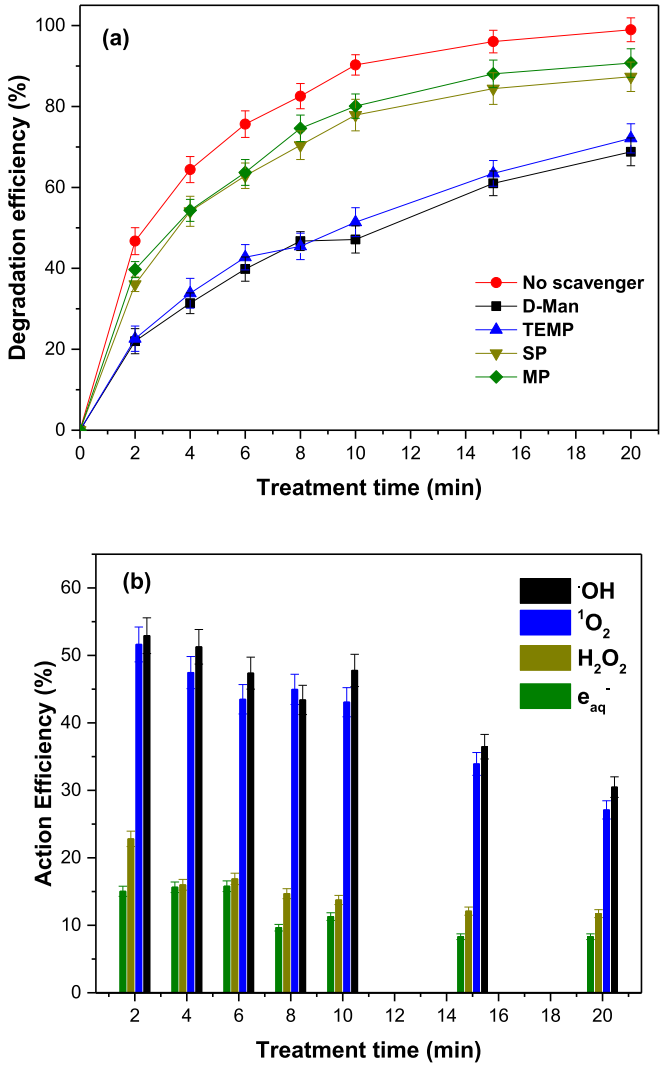

Fig. 6. (a) Effect of scavengers on the cephalexin degradation efficiency and (b) action efficiency of ·OH, $^1O_2$, H_2O_2 and e^-_{aq} species as a function of NSP-corona treatment time (pulse voltage: 24.2 kV; pulse frequency: 200 Hz; carrier gas: air; initial pollutant concentration: 40 mg/L).

scavenger (based on Eq. (4)) is also presented in Fig. 6b, clearly indicating the significant contribution of ·OH and $^1O_2$ in CPX degradation. During the early stages of NSP treatment (short treatment times), the action efficiency of both ·OH and $^1O_2$ was quite high (~52–53%) whereas those corresponding to H_2O_2 and e^-_{aq} were much lower; ~23% and ~15%, respectively. At the latter stages of NSP treatment (prolonged treatment times), the action efficiency of all investigated plasma RONS was significantly attenuated nevertheless the action efficiency of ·OH and $^1O_2$ remained significant (~31% and ~27%, respectively) while those of H_2O_2 and e^-_{aq}, revealed little contribution in the degradation process (~12% and ~8% respectively). Overall, D-man and TEMP had a much higher impact on CPX degradation efficiency compared to SP and MP, indicating the dominant role of the short-lived ·OH and $^1O_2$ in the degradation process compared to that of the hydrated plasma electrons and the long lived, albeit less reactive, H_2O_2.

3.6. NSP-corona towards degradation and mineralization of cephalosporin antibiotics

Next, we decided to evaluate the NSP efficiency towards the degradation of these two popular cephalosporins ; the comparison of degradation efficiency between cephalexin and cefazolin under the optimized conditions is illustrated in Fig. 7a. Obviously, the degradation efficiency of both CPX and CFZ gradually increased with NSP treatment time; after

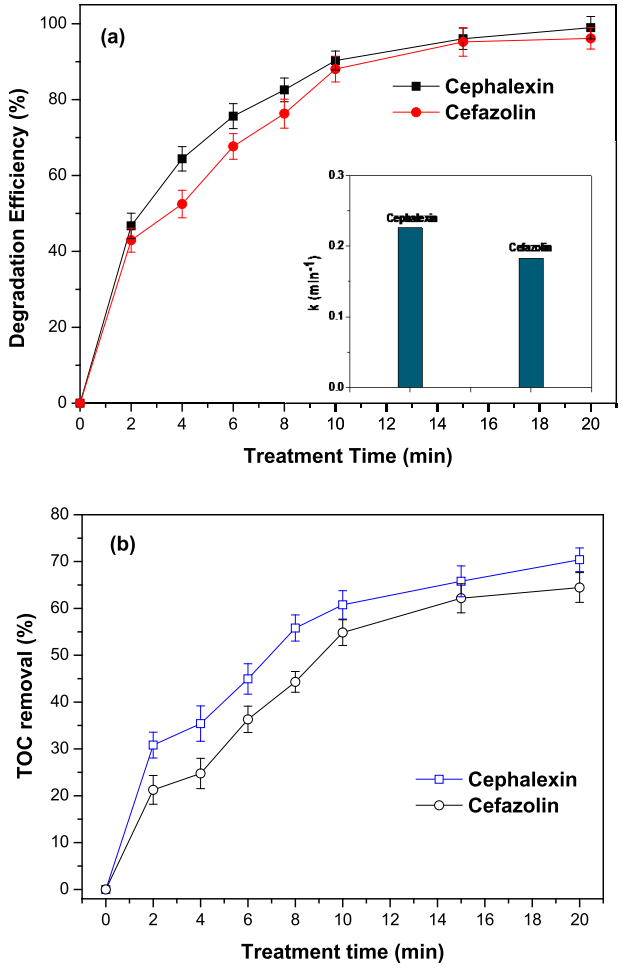

Fig. 7. Comparison between cephalexin and cefazolin with respect to their (a) degradation efficiencies as a function of NSP-corona treatment time (pseudo-first order degradation rates are shown in the inset) and (b) TOC removal as a function of NSP-corona treatment time (pulse voltage: 24.2 kV; pulse frequency: 200 Hz; carrier gas: air; initial pollutant concentration: 40 mg/L).

20 min of plasma treatment CPX was completely degraded (~99.0%) whereas the degradation of CFZ was only slightly less and equal to 96.1%. Under all treatment times, the degradation efficiencies ranked as CPX > CFZ followed first-order kinetic (section S5, Fig. S4) with the corresponding constants being 0.23 (CPX) and 0.18 min^{-1} (CFZ) suggesting that CPX is more vulnerable to plasma species than CFZ perhaps counterintuitively since the latter possesses more oxidizable sites including the additional sulfur atoms.

To assess cephalosporins mineralization, we measured the residual (after NSP treatment) organic content associated with CPX and CFZ trough TOC analysis and the results are shown in Fig. 7b. A high degree of TOC removal was achieved after 20 min of NSP treatment being 70.4% and 64.5% for CPX and CFZ, respectively. This TOC removal is higher than that achieved for the same pollutants with other AOPs (Table 2) and consistent with that achieved for cefixime antibiotic (i.e. 73.1%) after 30 min of treatment inside a plasma bubble reactor [32]. In line with degradation efficiencies, TOC removal also ranked as CPX > CFZ. Nevertheless, the TOC removal for both cephalosporins was lower compared to their degradation efficiency obtained from UV/Vis or HPLC analysis (section S4, Fig. S2) indicating the existence of intermediates which are resistant to further oxidation/degradation by plasma discharge. It is reminded here that HPLC was used to quantify the residual concentrations of the parent molecules, UV–Vis spectroscopy to investigate both the oxidation of parent molecules along with those with similar conjugate structures (absorb at near wavelengths) and TOC analysis for pollutants mineralization.

3.7. Cytotoxicity of the degraded CPX and CFZ solutions

We assessed the cytotoxicity of the CPX and CFZ solutions before and after plasma treatment towards MCF-7, MDA-MB-231 and U251MG glioblastoma cells. Treatment of the cells with untreated CPX and CFZ resulted in the reduction of cell viability (Fig. 8). In particular, the cell viability of MCF-7, MDA-MB-231 and U251MG after their incubation with untreated CPX solutions was measured ~ 85%, 73% and 88%, respectively. The corresponding cell viabilities for untreated CFZ solutions were even lower and determined as ~ 67%, 28% and 66%, respectively indicating the higher cytotoxicity of CFZ compared to CPX. However, when the CPX and CFZ solution at the same starting concentrations as those used for the cytotoxicity experiments above, where submitted to NSP-corona treatment, a significantly reduced cytotoxicity was detected as shown by the increased cell viability observed after exposure of both antibiotics to plasma (Fig. 8). Regarding CPX, the viability of all cell lines was higher than 95% after exposure to 10 min CAP whereas the 20 min plasma-treated CPX solutions had negligible toxicity since the viability of all investigated cells was identical to that of control samples (Fig. 8a). The toxicity of plasma-treated CFZ solutions

Table 2
Mineralization efficiency of cephalexin and cefazolin by various AOPs.

Method	Pollutant	Treatment time	TOC removal	Ref
NSP-corona	CPX, 40 mg/L	20 min	70.4%	This study
NSP-corona	CFZ, 40 mg/L	20 min	64.5%	This study
UV/sodium persulfate	CPX, 10 mg/L	60 min	52.3%	[71]
Fenton	CPX, 10 mg/L	60 min	59.6%	[71]
Ultrasonic waves/hydrogen peroxide/nickel oxide nanoparticles	CPX, 40 mg/L	90 min	54.55%	[72]
TiO_2-Photocatalysis	CFZ, 10 mg/L	240 min	36.0%	[73]
3D WO3-x/mesoporous carbon-Photocatalysis	CFZ, 1.4 mg/L	180 min	85.5%	[74]

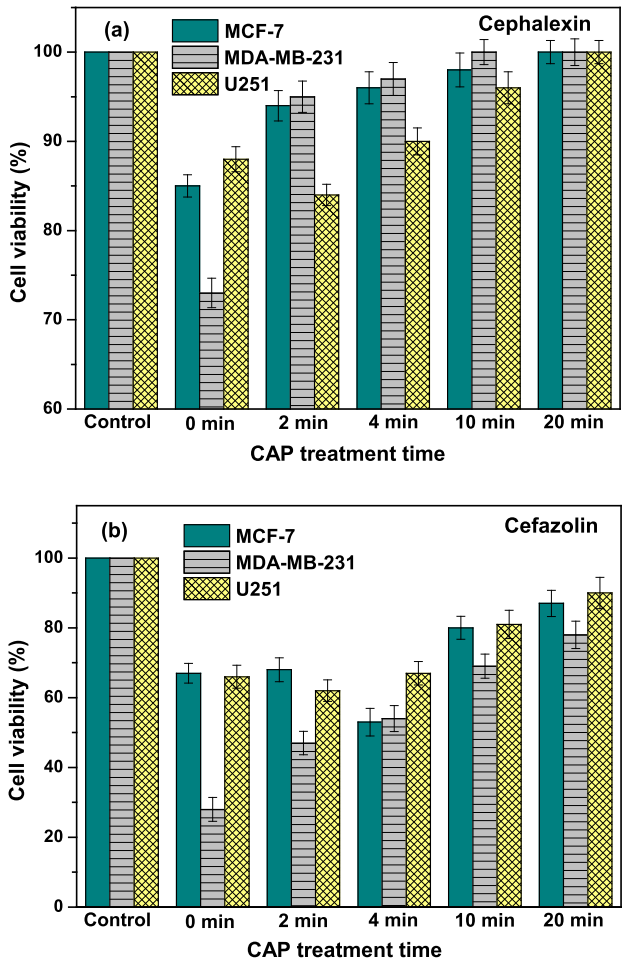

Fig. 8. Cytotoxicity towards MCF-7, MDA-MB-231 and U251MG glioblastoma cells of (a) cephalexin and (b) cefazolin solutions before and after plasma treatment (pulse voltage: 24.2 kV; pulse frequency: 200 Hz; carrier gas: air; initial pollutant concentration: 40 mg/L).

compared to untreated ones is illustrated in Fig. 8b. The viability of MDA-MB-231 cells was an increasing function of plasma treatment time; after 20 min the viability of MDA-MB-231 cells increased from 28% (untreated) to 78% whereas the viability of MCF-7 and U251MG cells increased from 67% and 66% (untreated) to 87% and 90%, respectively. It is noteworthy that for short treatment times (<4 min) the toxicity of CFZ towards MCF-7 and U251MG cells was enhanced as revealed by their reduced cell viability compared to the untreated CFZ solution (Fig. 8b). This suggests that upon plasma treatment certain initially formed intermediate(s) of CFZ exhibit higher overall toxicity (attributed either to their own or by the combination of more than one intermediates) than the parent CFZ which is in agreement with a recent study where short plasma treatment time of cefixime solution produced more toxic byproducts towards MCF-7 cells [32]. Therefore, prolonged plasma treatment may be required to ensure not only an efficient CFZ degradation but also an equally efficient degradation of toxic intermediates before an appropriately remediated aqueous solution is produced.

3.8. Identification of CPX and CFZ intermediates and degradation pathways

Several methods have been reported for the degradation of CPX contaminated solutions with varying degree of success. Notwithstanding to commend the effort in developing these methods, almost invariably, the interpretation of the associated data regarding CPX intermediates and degradation pathways proposed, are controversial and easily challenged on grounds of chemical reactivity fundamentals. In contrast, analogous reports on CFZ by several independent groups, are far more consistent and reasonable in terms of the structures of CFZ intermediates and degradation pathways proposed. Obviously, different methods give rise to different species therefore some diversity in the intermediates generated by any given pollutant is expected and in this type of studies one cannot assign a precise structure to each degradant unambiguously. Nevertheless, consistency with the chemical reactivity of the parent molecule cannot be ignored. We applied the broad and deep organic chemistry knowledge available in our team to propose structures that are consistent with HPLC polarity/retention times, MS fragmentation patterns and chemical reactivity towards oxidants rather than suggest structures that simply fit a molecular ion mass or lack chemical insight. More specifically we have adopted best practices exercised in the pharma industry when investigating drug metabolites (redox degradants and conjugates). Accordingly, all intermediates proposed are first and foremost consistent with established chemical transformations of each functional group and structural feature and subsequently were cross examined against the preliminary MS data. Whenever there was a lack of match, the proposed structures were revised, again according to the same assessment (HPLC polarity/retention time profile, MS fragmentation patterns and redox chemistry) until arrived at reasonable intermediates that could be connected mechanistically through established transformations.

In order to identify CPX and CFZ intermediates, we conducted a comprehensive analysis of UPLC/MS data from NSP-corona treated CPX and CFZ samples. Following analysis of the molecular ions in both positive and negative ionization modes and their fragmentation and isotope patterns, several species emerged as likely intermediates. These species were prioritized according to their relative abundance until a reasonable number of degradants and their fate became apparent. We also cross-checked the relative abundance of the molecular ions/proposed intermediates in a semi kinetic context, namely assessing the same species in samples from short, medium and long treatment times thus allowing to establish trends in the rise and fall of intermediates throughout the degradation process. It is also worth noting that this is the first report on plasma-induced degradation of CPX and CFZ hence insight of the chemical behavior of these antibiotics under plasma conditions could help further our understanding of the species and mechanisms involved in this process.

Analysis of UPLC/MS data from 10 min NSP-corona treated CPX aqueous solutions revealed the several intermediates that serve as witnesses to the reactions CPX had suffered. No intermediate was found where the β-lactam portion of the structure had survived, and this is consistent with the chemical and biochemical reactivity of this relatively labile functional group. The fate of the CPX intermediate resulting from hydrolysis of the *β*-lactam (CPX-HDR) appears to follow two main oxidative degradation pathways (Fig. 9a). In one fate (green set of intermediates) the benzylamine portion of the phenyl-glycine amide is oxidized to the imine (D 363A) followed by oxidation of the ring sulfide to the corresponding sulfoxide (D 379) consistent with the high propensity of these sites to be oxidized (cephalexin sulfoxide is itself commercially available). These oxidation events can be readily carried out by either $^1O_2$ or H_2O_2. Next, hydroxylation of the methyl group (most likely by ·H abstraction by ·OH and recombination of the resulting radical with ·OH) gives rise to alcohol intermediate D 395 which cyclizes to lactone D 260B after hydrolysis of the amide side chain and further oxidation of the sulfoxide to the sulfone. In this sub-pathway (green Fig. 9a), the loss of the amide side chain seems to govern the generation of lighter degradants whereas further oxidation of the lactone to the cyclic anhydride also manifests in D 260A.

In the other fate (purple, Fig. 9a) of CPX-HDR intermediate, the initial oxidation takes place on the ring by α-hydroxylation of the enamine and loss of water (hydroxylation by either $^1O_2$ or H_2O_2; see also conversion of D 360 to D 375C to D 357 in Fig. 9b), resulting in its

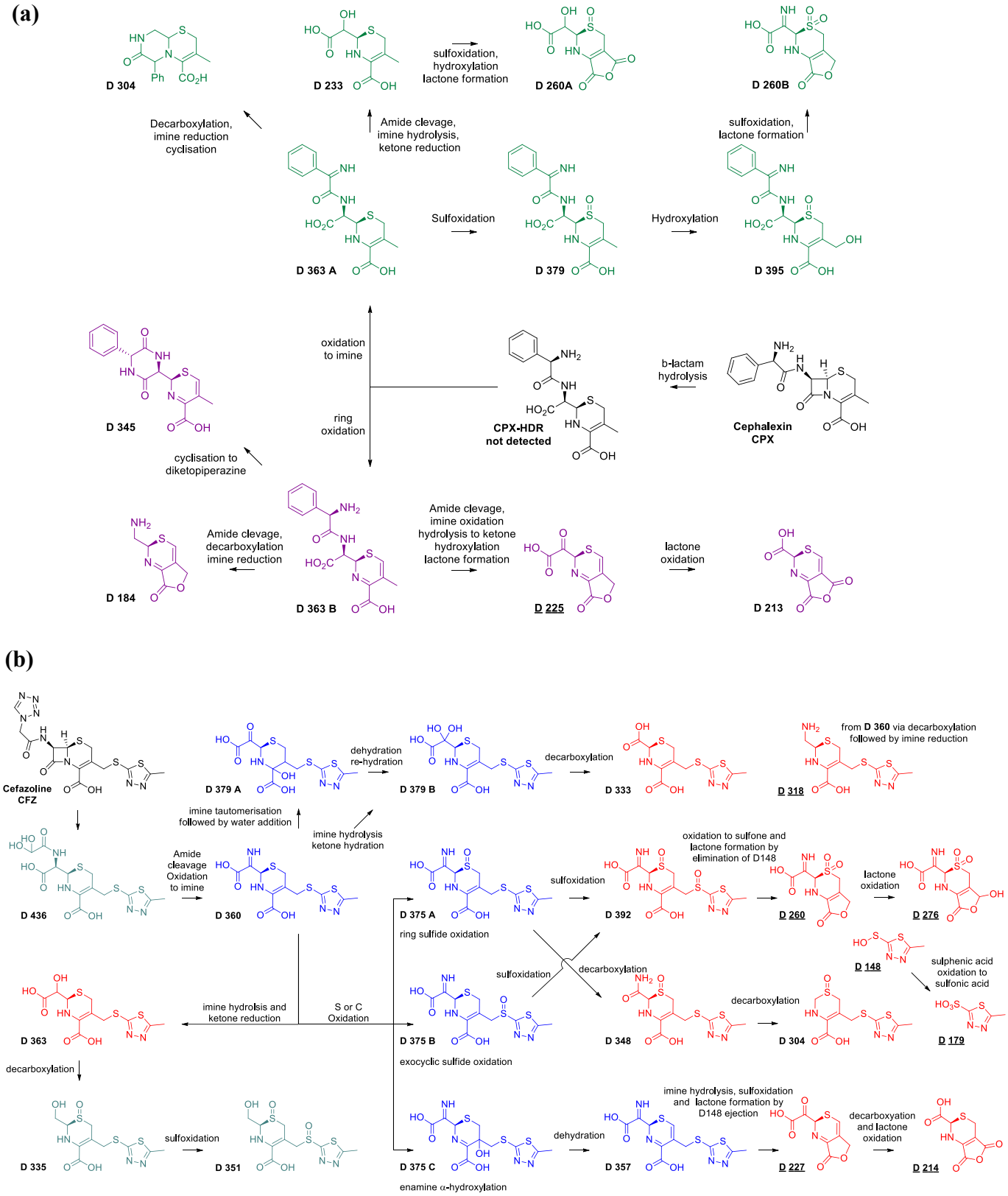

Fig. 9. Proposed plasma-induced degradation pathways of (a) cephalexin and (b) cefazolin (Red set: Late/persisting degradants even after 20 min of NSP-corona treatment time. Blue set: Early degradants at 4–8 min treatment time). The numbers correspond to the molecular weight of the intermediates. Underlined are those detected in the negative ionization mode; all others were detected in the protonated form (+ve mode). (For interpretation of the references to colour in this figure legend, the reader is referred to the web version of this article.)

dehydrogenation to the thiazine derivative D 363B. This renders the sulfur atom vinylic hence conjugated and much less reactive towards oxidation whereas the attached methyl group becomes more (benzylic-like) prone to ·OH mediated hydroxylation. In fact, this sub-pathway (purple, Fig. 9a) appears to be driven by methyl hydroxylation as all downstream lighter fragments relate to the corresponding lactone and/or anhydride retaining the sulfur atom unoxidized. The same intermediates were observed in the 20 min treated CPX solutions albeit at lesser intensities/amounts suggesting increased resistance to further oxidation and undoubtedly are the main contributors to the residual TOC.

CFZ aqueous solutions after 10 min of CAP treatment were also interrogated and several intermediates were found (structures in red colour in Fig. 9b) which in turn are consistent with the action efficiencies of the ROS species determined above ($^1O_2$ and ·OH being the main drivers of the degradation followed by H_2O_2 and electron transfer processes). Interestingly, the 1,3,4-thiadiazole ring is retained intact in most of these intermediates which is consistent with its reduced nucleophilic character therefore reduced tendency to react with electrophilic O reagents ($^1O_2$ or H_2O_2) and become oxidized. These intermediates persist, albeit to a lesser degree, even after 20 min of treatment thus contributing to the residual TOC. Given the increased cytotoxicity manifested for treated CFZ solutions for short times, we investigated earlier intermediates in order to identify potentially toxic early intermediates and also to uncover more of the CFZ degradation pathway. Thus, we interrogated CFZ solutions subjected to 4–8 min of treatment and found more intermediates (blue set of compounds in Fig. 9b) that are reasonable precursors to the persisting degradants identified at 10–20 min of treatment time (red set of compounds in Fig. 9b). In this way a comprehensive degradation map of the CFZ plasma-induced fate was constructed which makes chemical sense and is consistent both with the relative action efficiencies of the ROS species involved and our established understanding of the plasma-induced degradation reactions studied on other pollutants [37,38].

4. Conclusions

A nanosecond pulsed multi-pin-to-liquid corona discharge plasma reactor resulted in complete and high energy-efficient degradation of cephalexin and cefazolin in water with the maximum calculated energy yield (i.e. 1.37 g/kWh) being about two orders of magnitude higher than that reported in other studies. Increased pulse voltage led to an increased RONS concentration in water, enhancing the degradation of cephalosporins. CPX degradation rate was slower at higher pollutant concentrations and also in tap water compared to that in 3D water. Under the various plasma atmospheres, different RONS were generated both at the plasma gas phase and inside the water, affecting the degradation of cephalosporins in the order O_2 > air > N_2. O_2-plasma produced much higher H_2O_2 concentrations but not any NO_2^-/NO_3^- species compared to air and N_2-plasmas where the generation of the aforementioned RNS caused a serious decrease of solution pH. Experiments with a range of specific scavengers, suggested that cephalosporins degradation is mediated primarily by $^{\cdot}OH$ and $^1O_2$ as evidenced by their significant action efficiency (~52–53%) whereas the contribution of H_2O_2 and hydrated plasma electrons was substantially lower (~23% and ~15%). However, the almost equal degradation efficiencies between air- and O_2-plasma are indicative of the significant contribution of some RNS (e.g. ONOOH/$ONOO^-$) generated in air-plasma. Higher degradation efficiency and TOC removal was achieved for CPX in comparison to CFZ although both were reasonably well degraded. The degradation pathways for both CPX and CFZ involved mainly hydroxylation decarboxylation, sulfoxidation and dehydrogenation reactions leading at higher plasma treatment times to intermediates with zero or low toxicity as indicated by the increased human cell viability for CPX/CFZ contaminated water post plasma-treatment. This study provides useful insights and potential development/scale-up of the present CAP system as one of the most efficient and sustainable remediation approaches for antibiotic-polluted wastewater. Our future research steps will focus on the exploitation of CAP for the remediation of water polluted by different types of emerging contaminants (e.g. polyfluorinated alkyl substances, PFAS).

CRediT authorship contribution statement

S. Meropoulis: Methodology, Investigation, Visualization. **S. Giannoulia:** Methodology, Investigation, Visualization. **S. Skandalis:** Methodology, Investigation. **G. Rassias:** Methodology, Investigation, Writing – review & editing. **C.A. Aggelopoulos:** Conceptualization, Methodology, Investigation, Visualization, Supervision, Resources, Writing – original draft, Writing – review & editing, Funding acquisition.

Declaration of Competing Interest

The authors declare that they have no known competing financial interests or personal relationships that could have appeared to influence the work reported in this paper.

Acknowledgements

This project has received funding from the Hellenic Foundation for Research and Innovation (HFRI) under grant agreement No [3560] and from the European Union's Horizon 2020 research and innovation programme under grant agreement No101037509. We wish to cordially thank Dr. V. Bekiari and Dr. D. Tataraki for their invaluable help concerning the TOC measurements and quantitative determination of residual antibiotics by HPLC.

Appendix A. Supplementary material

Supplementary data to this article can be found online at https://doi.org/10.1016/j.seppur.2022.121639.

References

[1] S. Sengupta, M. Chattopadhyay, H.-P. Grossart, The multifaceted roles of antibiotics and antibiotic resistance in nature. *Frontiers in Microbiology*, **4** (2013) ar. no. 47.
[2] A.B.A. Boxall, P. Johnson, E.J. Smith, C.J. Sinclair, E. Stutt, L.S. Levy, Uptake of Veterinary Medicines from Soils into Plants, J. Agric. Food. Chem. 54 (6) (2006) 2288–2297.
[3] P. Westerhoff, Y. Yoon, S. Snyder, E. Wert, Fate of Endocrine-Disruptor, Pharmaceutical, and Personal Care Product Chemicals during Simulated Drinking Water Treatment Processes, Environ. Sci. Technol. 39 (17) (2005) 6649–6663.
[4] P.A. Bradford, Extended-Spectrum β-Lactamases in the 21st Century: Characterization, Epidemiology, and Detection of This Important Resistance Threat, Clin. Microbiol. Rev. 14 (4) (2001) 933–951.
[5] F.C. Tenover, Mechanisms of Antimicrobial Resistance in Bacteria, The American Journal of Medicine 119 (2006) S3–S10.
[6] A.O. Adekanmbi, M.O. Akinpelu, A.V. Olaposi, A.A. Oyelade, Diversity of Extended Spectrum Beta-lactamase (ESBL) genes in Escherichia coli isolated from wastewater generated by a Sick Bay located in a University Health Care Facility, Gene Reports 20 (2020), 100738.
[7] Y. Pfeifer, A. Cullik, W. Witte, Resistance to cephalosporins and carbapenems in Gram-negative bacterial pathogens, Int. J. Med. Microbiol. 300 (6) (2010) 371–379.
[8] K. Kümmerer, Antibiotics in the aquatic environment – A review – Part I, Chemosphere 75 (4) (2009) 417–434.
[9] D. Dalen, A. Fry, S.G. Campbell, J. Eppler, P.J. Zed, Intravenous cefazolin plus oral probenecid versus oral cephalexin for the treatment of skin and soft tissue infections: a double-blind, non-inferiority, randomised controlled trial, Emergency Medicine Journal 35 (8) (2018) 492–498.
[10] A.J. Watkinson, E.J. Murby, D.W. Kolpin, S.D. Costanzo, The occurrence of antibiotics in an urban watershed: From wastewater to drinking water, Sci. Total Environ. 407 (8) (2009) 2711–2723.
[11] A.L. Demain, R.B. Walton, J.F. Newkirk, I.M. Miller, Microbial Degradation of Cephalosporin C, Nature 199 (4896) (1963) 909–910.
[12] See https://ec.europa.eu/environment/soil/soil_policy_en.htm.
[13] Y. Deng, R. Zhao, Advanced Oxidation Processes (AOPs) in Wastewater Treatment, Current Pollution Reports 1 (3) (2015) 167–176.

[14] F. Biancullo, N.F.F. Moreira, A.R. Ribeiro, C.M. Manaia, J.L. Faria, O.C. Nunes, S. M. Castro-Silva, A.M.T. Silva, Heterogeneous photocatalysis using UVA-LEDs for the removal of antibiotics and antibiotic resistant bacteria from urban wastewater treatment plant effluents, Chem. Eng. J. 367 (2019) 304–313.
[15] I.C. Iakovides, I. Michael-Kordatou, N.F.F. Moreira, A.R. Ribeiro, T. Fernandes, M. F.R. Pereira, O.C. Nunes, C.M. Manaia, A.M.T. Silva, D. Fatta-Kassinos, Continuous ozonation of urban wastewater: Removal of antibiotics, antibiotic-resistant Escherichia coli and antibiotic resistance genes and phytotoxicity, Water Res. 159 (2019) 333–347.
[16] L. Chu, D. Chen, J. Wang, Z. Yang, Q.i. Yang, Y. Shen, Degradation of antibiotics and inactivation of antibiotic resistance genes (ARGs) in Cephalosporin C fermentation residues using ionizing radiation, ozonation and thermal treatment, J. Hazard. Mater. 382 (2020), 121058.
[17] Y. Qian, G. Xue, J. Chen, J. Luo, X. Zhou, P. Gao, Q.i. Wang, Oxidation of cefalexin by thermally activated persulfate: Kinetics, products, and antibacterial activity change, J. Hazard. Mater. 354 (2018) 153–160.
[18] C.A. Aggelopoulos, Recent advances of cold plasma technology for water and soil remediation: A critical review, Chem. Eng. J. 428 (2022), 131657.
[19] C.A. Aggelopoulos, Atmospheric pressure dielectric barrier discharge for the remediation of soil contaminated by organic pollutants, Int. J. Environ. Sci. Technol. 13 (7) (2016) 1731–1740.
[20] R.C. Sanito, S.-J. You, Y.-F. Wang, Degradation of contaminants in plasma technology: An overview, J. Hazard. Mater. 424 (2022), 127390.
[21] Y. Zheng, S. Wu, J. Dang, S. Wang, Z. Liu, J. Fang, P. Han, J. Zhang, Reduction of phoxim pesticide residues from grapes by atmospheric pressure non-thermal air plasma activated water, J. Hazard. Mater. 377 (2019) 98–105.
[22] C.A. Aggelopoulos, C.D. Tsakiroglou, A new perspective towards in-situ cold plasma remediation of polluted sites: Direct generation of micro-discharges within contaminated medium, Chemosphere 266 (2021), 128969.
[23] E.S.M. Mouele, J.O. Tijani, K.O. Badmus, O. Pereao, O. Babajide, O.O. Fatoba, C. Zhang, T. Shao, E. Sosnin, V. Tarasenko, K. Laatikainen, L.F. Petrik, A critical review on ozone and co-species, generation and reaction mechanisms in plasma induced by dielectric barrier discharge technologies for wastewater remediation, J. Environ. Chem. Eng. 9 (5) (2021), 105758.
[24] N. Hojnik, M. Modic, J.L. Walsh, D. Žigon, U. Javornik, J. Plavec, B. Žegura, M. Filipič, U. Cvelbar, Unravelling the pathways of air plasma induced aflatoxin B1 degradation and detoxification, J. Hazard. Mater. 403 (2021), 123593.
[25] K.-S. Kim, C.-S. Yang, Y.S. Mok, Degradation of veterinary antibiotics by dielectric barrier discharge plasma, Chem. Eng. J. 219 (2013) 19–27.
[26] H. Li, T. Li, S. He, J. Zhou, T. Wang, L. Zhu, Efficient degradation of antibiotics by non-thermal discharge plasma: Highlight the impacts of molecular structures and degradation pathways, Chem. Eng. J. 395 (2020), 125091.
[27] Q. Zhang, H. Zhang, Q. Zhang, Q. Huang, Degradation of norfloxacin in aqueous solution by atmospheric-pressure non-thermal plasma: Mechanism and degradation pathways, Chemosphere 210 (2018) 433–439.
[28] P.T.T. Nguyen, H.T. Nguyen, U.N.P. Tran, H.a. Manh Bui, A. Aldawsari, Removal of Antibiotics from Real Hospital Wastewater by Cold Plasma Technique, J. Chem. 2021 (2021) 1–13.
[29] X. Gao, K. Huang, A. Zhang, C. Wang, Z. Sun, Y. Liu, Simultaneous degradation of glucocorticoids and sterilization using bubbling corona discharge plasma based systems: a promising terminal water treatment facility for hospital wastewater, Chem. Eng. J. 132845 (2021).
[30] M. Magureanu, F. Bilea, C. Bradu, D. Hong, A review on non-thermal plasma treatment of water contaminated with antibiotics, J. Hazard. Mater. 417 (2021), 125481.
[31] K. Shang, R. Morent, N. Wang, Y. Wang, B. Peng, N. Jiang, N.a. Lu, J. Li, Degradation of sulfamethoxazole (SMX) by water falling film DBD Plasma/Persulfate: Reactive species identification and their role in SMX degradation, Chem. Eng. J. 431 (2022), 133916.
[32] T. Zhang, R. Zhou, P. Wang, A. Mai-Prochnow, R. McConchie, W. Li, R. Zhou, E. W. Thompson, K.(. Ostrikov, P.J. Cullen, Degradation of cefixime antibiotic in water by atmospheric plasma bubbles: Performance, degradation pathways and toxicity evaluation, Chem. Eng. J. 421 (2021), 127730.
[33] M.A. Malik, Water Purification by Plasmas: Which Reactors are Most Energy Efficient? Plasma Chem. Plasma Process. 30 (1) (2010) 21–31.
[34] B.o. Jiang, J. Zheng, S. Qiu, M. Wu, Q. Zhang, Z. Yan, Q. Xue, Review on electrical discharge plasma technology for wastewater remediation, Chem. Eng. J. 236 (2014) 348–368.
[35] J. Ren, T. Wang, G. Qu, D. Liang, S. Hu, Evaluation and Optimization of Electrode Configuration of Multi-Channel Corona Discharge Plasma for Dye-Containing Wastewater Treatment, Plasma Sci. Technol 17 (12) (2015) 1053–1060.
[36] M. Magureanu, D. Piroi, N.B. Mandache, V. David, A. Medvedovici, V.I. Parvulescu, Degradation of pharmaceutical compound pentoxifylline in water by non-thermal plasma treatment, Water Res. 44 (11) (2010) 3445–3453.
[37] S. Meropoulis, G. Rassias, V. Bekiari, C.A. Aggelopoulos, Structure-Degradation efficiency studies in the remediation of aqueous solutions of dyes using nanosecond-pulsed DBD plasma, Sep. Purif. Technol. 274 (2021), 119031.
[38] C.A. Aggelopoulos, S. Meropoulis, M. Hatzisymeon, Z.G. Lada, G. Rassias, Degradation of antibiotic enrofloxacin in water by gas-liquid nsp-DBD plasma: Parametric analysis, effect of H2O2 and CaO2 additives and exploration of degradation mechanisms, Chem. Eng. J. 398 (2020), 125622.
[39] H.e. Guo, N. Jiang, H. Wang, N.a. Lu, K. Shang, J. Li, Y. Wu, Pulsed discharge plasma assisted with graphene-WO3 nanocomposites for synergistic degradation of antibiotic enrofloxacin in water, Chem. Eng. J. 372 (2019) 226–240.
[40] W. Zhang, H. Gao, J. He, P. Yang, D. Wang, T. Ma, H. Xia, X. Xu, Removal of norfloxacin using coupled synthesized nanoscale zero-valent iron (nZVI) with H2O2 system: Optimization of operating conditions and degradation pathway, Sep. Purif. Technol. 172 (2017) 158–167.
[41] Y. Liu, C. Wang, K. Huang, A.C. Miruka, A.i. Dong, Y. Guo, A.i. Zhang, Degradation of glucocorticoids in water by dielectric barrier discharge and dielectric barrier discharge combined with calcium peroxide: performance comparison and synergistic effects, J. Chem. Technol. Biotechnol. 94 (11) (2019) 3606–3617.
[42] H. Zeghioud, P. Nguyen-Tri, L. Khezami, A. Amrane, A.A. Assadi, Review on discharge Plasma for water treatment: mechanism, reactor geometries, active species and combined processes, J. Water Process Eng. 38 (2020), 101664.
[43] M. Hatzisymeon, D. Tataraki, C. Tsakiroglou, G. Rassias, C.A. Aggelopoulos, Highly energy-efficient degradation of antibiotics in soil: Extensive cold plasma discharges generation in soil pores driven by high voltage nanopulses, Sci. Total Environ. 786 (2021), 147420.
[44] M. Hatzisymeon, D. Tataraki, G. Rassias, C.A. Aggelopoulos, Novel combination of high voltage nanopulses and in-soil generated plasma micro-discharges applied for the highly efficient degradation of trifluralin, J. Hazard. Mater. 415 (2021), 125646.
[45] C.A. Aggelopoulos, M. Hatzisymeon, D. Tataraki, G. Rassias, Remediation of ciprofloxacin-contaminated soil by nanosecond pulsed dielectric barrier discharge plasma: Influencing factors and degradation mechanisms, Chem. Eng. J. 393 (2020), 124768.
[46] P. Jamróz, P. Pohl, W. Żyrnicki, Spectroscopic evaluation of a low power atmospheric pressure mixed argon–helium microwave induced plasma combined with the chemical generation of volatile species for the optical emission spectrometric determination of arsenic, antimony and mercury, J. Anal. At. Spectrom. 27 (2012) 1772–1779.
[47] R. Zhou, R. Zhou, P. Wang, B. Luan, X. Zhang, Z. Fang, Y. Xian, X. Lu, K. K. Ostrikov, K. Bazaka, Microplasma Bubbles: Reactive Vehicles for Biofilm Dispersal, ACS Appl. Mater. Interfaces 11 (23) (2019) 20660–20669.
[48] F. Rezaei, M. Abbasi-Firouzjah, B. Shokri, Investigation of antibacterial and wettability behaviours of plasma-modified PMMA films for application in ophthalmology, J. Phys. D Appl. Phys. 47 (8) (2014), 085401.
[49] D.K. Yadav, M. Adhikari, S. Kumar, B. Ghimire, I. Han, M.-H. Kim, E.-H. Choi, Cold atmospheric plasma generated reactive species aided inhibitory effects on human melanoma cells: an in vitro and in silico study, Sci. Rep. 10 (1) (2020).
[50] S. Wang, Z. Zhou, R. Zhou, Z. Fang, P.J. Cullen, Effect of solution pH on the characteristics of pulsed gas–liquid discharges and aqueous reactive species in atmospheric air, J. Appl. Phys. 130 (10) (2021), 103302.
[51] R. Dawson, J. Little, Characterization of nanosecond pulse driven dielectric barrier discharge plasma actuators for aerodynamic flow control, J. Appl. Phys. 113 (10) (2013), 103302.
[52] J.-P. Liang, X.-F. Zhou, Z.-L. Zhao, D.-Z. Yang, W.-C. Wang, Degradation of trimethoprim in aqueous by persulfate activated with nanosecond pulsed gas-liquid discharge plasma, J. Environ. Manage. 278 (2021), 111539.
[53] R.K. Singh, L. Philip, S. Ramanujam, Rapid degradation, mineralization and detoxification of pharmaceutically active compounds in aqueous solution during pulsed corona discharge treatment, Water Res. 121 (2017) 20–36.
[54] N.M. Shooshtari, M.M. Ghazi, An investigation of the photocatalytic activity of nano α-Fe2O3/ZnO on the photodegradation of cefixime trihydrate, Chem. Eng. J. 315 (2017) 527–536.
[55] Y.Y. Gurkan, N. Turkten, A. Hatipoglu, Z. Cinar, Photocatalytic degradation of cefazolin over N-doped TiO2 under UV and sunlight irradiation: Prediction of the reaction paths via conceptual DFT, Chem. Eng. J. 184 (2012) 113–124.
[56] M. Aram, M. Farhadian, A.R. Solaimany Nazar, S. Tangestaninejad, P. Eskandari, B.-H. Jeon, Metronidazole and Cephalexin degradation by using of Urea/TiO2/ZnFe2O4/Clinoptiloite catalyst under visible-light irradiation and ozone injection, J. Mol. Liq. 304 (2020), 112764.
[57] J. He, Y. Zhang, Y. Guo, G. Rhodes, J. Yeom, H. Li, et al., Photocatalytic degradation of cephalexin by ZnO nanowires under simulated sunlight: Kinetics, influencing factors, and mechanisms, Environ. Int. 132 (2019), 105105.
[58] X. Liu, C. Ma, Y. Yan, G. Yao, Y. Tang, P. Huo, W. Shi, Y. Yan, Hydrothermal Synthesis of CdSe Quantum Dots and Their Photocatalytic Activity on Degradation of Cefalexin, Ind. Eng. Chem. Res. 52 (43) (2013) 15015–15023.
[59] M. Laroussi, F. Leipold, Evaluation of the roles of reactive species, heat, and UV radiation in the inactivation of bacterial cells by air plasmas at atmospheric pressure, Int. J. Mass Spectrom. 233 (1-3) (2004) 81–86.
[60] B.R. Locke, K.-Y. Shih, Review of the methods to form hydrogen peroxide in electrical discharge plasma with liquid water, Plasma Sources Sci. Technol. 20 (3) (2011), 034006.
[61] W.V. Gaens, A. Bogaerts, Kinetic modelling for an atmospheric pressure argon plasma jet in humid air, J. Phys. D Appl. Phys. 46 (27) (2013), 275201.
[62] C. Fang, S. Wang, H. Xu, Q. Huang, Degradation of tetracycline by atmospheric-pressure non-thermal plasma: Enhanced performance, degradation mechanism, and toxicity evaluation, Sci. Total Environ. 812 (2022), 152455.
[63] B.M. Cadorin, V.D. Tralli, E. Ceriani, L.O.d.B. Benetoli, E. Marotta, C. Ceretta, N. A. Debacher, C. Paradisi, Treatment of methyl orange by nitrogen non-thermal plasma in a corona reactor: The role of reactive nitrogen species, J. Hazard. Mater. 300 (2015) 754–764.
[64] D.X. Liu, Z.C. Liu, C. Chen, A.J. Yang, D. Li, M.Z. Rong, H.L. Chen, M.G. Kong, Aqueous reactive species induced by a surface air discharge: Heterogeneous mass transfer and liquid chemistry pathways, Sci. Rep. 6 (1) (2016).
[65] W. Li, R. Zhou, R. Zhou, J. Weerasinghe, T. Zhang, A. Gissibl, et al., Insights into amoxicillin degradation in water by non-thermal plasmas, Chemosphere (2021) 132757.

[66] C. Bradu, K. Kutasi, M. Magureanu, N. Puač, S. Živković, Reactive nitrogen species in plasma-activated water: generation, chemistry and application in agriculture, J. Phys. D Appl. Phys. 53 (22) (2020), 223001.
[67] M.-C. Danner, A. Robertson, V. Behrends, J. Reiss, Antibiotic pollution in surface fresh waters: Occurrence and effects, Sci. Total Environ. 664 (2019) 793–804.
[68] C.A. Aggelopoulos, D. Tataraki, G. Rassias, Degradation of atrazine in soil by dielectric barrier discharge plasma – Potential singlet oxygen mediation, Chem. Eng. J. 347 (2018) 682–694.
[69] Y. Liu, C. Wang, X. Shen, A.i. Zhang, S. Yan, X. Li, A.C. Miruka, S. Wu, Y. Guo, S. Ognier, Degradation of glucocorticoids in aqueous solution by dielectric barrier discharge: Kinetics, mechanisms, and degradation pathways, Chem. Eng. J. 374 (2019) 412–428.
[70] R. Zhou, T. Zhang, R. Zhou, A. Mai-Prochnow, S.B. Ponraj, Z. Fang, H. Masood, J. Kananagh, D. McClure, D. Alam, K.(. Ostrikov, P.J. Cullen, Underwater microplasma bubbles for efficient and simultaneous degradation of mixed dye pollutants, Sci. Total Environ. 750 (2021), 142295.
[71] A. Almasi, R. Esmaeilpoor, H. Hoseini, V. Abtin, M. Mohammadi, Photocatalytic degradation of cephalexin by UV activated persulfate and Fenton in synthetic wastewater: optimization, kinetic study, reaction pathway and intermediate products, Journal of Environmental Health Science and Engineering 18 (2) (2020) 1359–1373.
[72] A. Seid-Mohammadi, G. Asgarai, Z. Ghorbanian, A. Dargahi, The removal of cephalexin antibiotic in aqueous solutions by ultrasonic waves/hydrogen peroxide/nickel oxide nanoparticles (US/H2O2/NiO) hybrid process, Sep. Sci. Technol. 55 (8) (2020) 1558–1568.
[73] K.K. Abbas, K.M. Shabeeb, A.A.A. Aljanabi, A.M.H.A. Al-Ghaban, Photocatalytic degradation of Cefazolin over spherical nanoparticles of TiO2/ZSM-5 mesoporous nanoheterojunction under simulated solar light, Environ. Technol. Innovation 20 (2020), 101070.
[74] P. Gholami, A. Khataee, A. Bhatnagar, Photocatalytic degradation of antibiotic and hydrogen production using diatom-templated 3D WO3-x@mesoporous carbon nanohybrid under visible light irradiation, Journal of Cleaner Production 275 (2020), 124157.